Structural Requirements for Drug Inhibition of the Liver Specific Human Organic Cation Transport Protein 1

Gustav Ahlin,[†] Johan Karlsson,[‡] Jenny M. Pedersen,[†] Lena Gustavsson,[§] Rolf Larsson,[||] Pär Matsson,[†] Ulf Norinder,[⊥] Christel A. S. Bergström,[†] and Per Artursson*[,†]

Pharmaceutical Screening and Informatics, Department of Pharmacy and Cancer Pharmacology and Informatics, Department of Medical Sciences, Uppsala University, Sweden, and AstraZeneca R&D, Mölndal, Lund, and Södertälje, Sweden

Received March 20, 2008

The liver-specific organic cation transport protein (OCT1; SLC22A1) transports several cationic drugs including the antidiabetic drug metformin and the anticancer agents oxaliplatin and imatinib. In this study, we explored the chemical space of registered oral drugs with the aim of studying the inhibition pattern of OCT1 and of developing predictive computational models of OCT1 inhibition. In total, 191 structurally diverse compounds were examined in HEK293-OCT1 cells. The assay identified 47 novel inhibitors and confirmed 15 previously known inhibitors. The enrichment of OCT1 inhibitors was seen in several drug classes including antidepressants. High lipophilicity and a positive net charge were found to be the key physicochemical properties for OCT1 inhibition, whereas a high molecular dipole moment and many hydrogen bonds were negatively correlated to OCT1 inhibition. The data were used to generate OPLS-DA models for OCT1 inhibitors; the final model correctly predicted 82% of the inhibitors and 88% of the noninhibitors of the test set.

Introduction

At physiological pH, 40% of all drugs are cations,[1] several of which are cleared from the blood by active transport into the hepatocytes in the liver. The organic cation transporter 1 (OCT1[a]; SLC22A1), is an integral membrane protein that transports cationic drugs[2] and is highly expressed in the liver.[3−6] Other members of the OCT gene family mediate drug transport in the kidney (OCT2)[3] and in many other organs (OCT3).[7] Important drugs that are dependent on OCT1-mediated uptake include the antidiabetic drug metformin and anticancer agents such as oxaliplatin and imatinib.[8−10] Several other drugs have been identified as OCT1 inhibitors.[4,11,12] The expression of OCT1 in six different colon cancer cell lines, in a number of colon cancer samples,[9] and in six noncolon cancer cell lines[12] suggests that OCT1 also is directly involved in drug uptake in cancer cells. These examples indicate that human OCT1 has a strong influence on the pharmaco- and toxicokinetics of many cationic drugs and that competition for OCT1 binding and transport may result in drug−drug interactions. Therefore, we were interested in investigating the molecular features that influence the binding of drugs and druglike molecules to human OCT1.

An examination of the literature revealed that a variety of experimental systems have been used to study OCT1 inhibition.[4,11,12] Because the heterogeneity of these assays makes it difficult to compare the results, we developed a new assay that has the capacity to screen a large number of compounds for OCT1 inhibition.[13] With this assay, we identified 47 new OCT1 inhibitors within the drug space of registered oral drugs.[14] The experimental data were used to develop easily interpretable qualitative models that predicted OCT1 inhibition with good precision based on a single inhibitor concentration. The experimental data were used to develop easily interpretable qualitative models that predicted OCT1 inhibition with good precision. The best model correctly predicted 82% of the OCT1 inhibitors and 88% of the noninhibitors in the test set and identified a number of molecular requirements for OCT1 inhibition. We emphasize that the devised models that are based on a single inhibitor concentration are limited to qualitative predictions of OCT1 inhibition. Attempts to develop pharmacophore models for more quantitative predictions on the basis of K_i values were not successful.

Results

OCT1 Inhibition Assay. The background activity of endogenous transport proteins and enzymes can reduce the specificity of overexpressed transport proteins such as OCT1.[15,16] With the intention of investigating the OCT1 specificity in our assay, we characterized the gene expression of 36 transport proteins, including OCT1, and 6 enzymes that are known to be important for drug disposition in HEK (human embryonic kidney)-OCT1 and HEK empty vector cells (as displayed in Figure 1a with Supporting Information in Table S1). In general, HEK-OCT1 cells expressed OCT1 levels that were more than 100 times higher than those of 34 of the other transport proteins and 6 enzymes investigated. The only exception was the level of monocarboxylate transporter 1 (MCT1; SLC16A1), which was 11 times lower than that for OCT1 (Figure 1a). In comparison, the empty-vector-transfected cells expressed almost no OCT1, whereas the background expression of other transport proteins and enzymes was comparable to that of the OCT1-transfected cells, as displayed in the Supporting InformationTable S1. Because the transport of 4-(4-(dimethylamino)styryl)-*N*-methylpyridinium (ASP^+) by the HEK-OCT1 cells was 12 times greater than that by the empty-vector-transfected cells (Figure 1b), we conclude that HEK-

* To whom correspondence should be addressed: Address: Pharmaceutical Screening and Informatics, Department of Pharmacy, Uppsala University, P.O. Box 580, SE-751 23 Uppsala, Sweden. Tel: +46-18-471 44 71. Fax: +46-18-471 44 84. E-mail: Per.Artursson@farmaci.uu.se.

[†] Department of Pharmacy, Uppsala University.

[‡] AstraZeneca R&D, Mölndal, Sweden.

[§] AstraZeneca R&D, Lund, Sweden.

[||] Department of Medical Sciences, Uppsala University.

[⊥] AstraZeneca R&D, Södertälje, Sweden.

[a] Abbreviations: ABC, ATP-binding cassette; ASP^+, 4-(4-(dimethylamino)styryl)-*N*-methylpyridinium; BCRP, breast cancer resistance protein; ClogP, octanol−water partition coefficient; DMSO, dimethyl sulfoxide; RFU, relative fluorescence units; HBSS, Hank's balanced salt solution; HEK293, human embryonic kidney suspension cells; MRP, multidrug resistance protein; OCT, organic cation transport protein; OPLS-DA, orthogonal partial least-squares projection to latent structures discriminant analysis; PBS, phosphate-buffered saline; PCA, principal component analysis; PCR, polymerase chain reaction; SLC, solute carrier.

10.1021/jm8003152 CCC: $40.75
Published on Web 09/13/2008

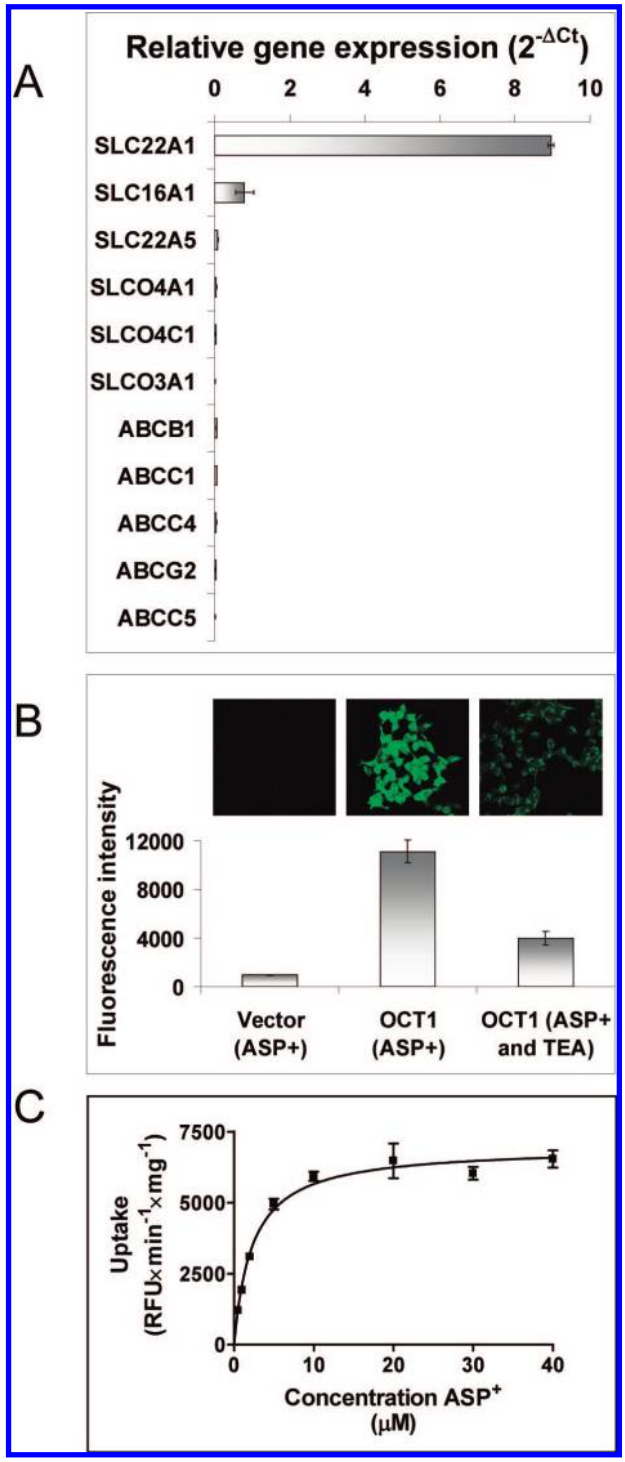

Figure 1. (A) Gene expression profile for the HEK293 cells transfected with OCT1 (SLC22A1). The cells overexpress OCT1, whereas the background expression of other transport proteins is low. Only the 10 transport proteins with the highest mRNA expression, defined as a relative expression larger than 0.01, are shown. None of the six CYP enzymes that were investigated had a relative mRNA expression that was above 0.01. The expression levels of all 36 transport proteins and 6 enzymes investigated are given in the Supporting Information Table S1. (B) The images show the uptake of ASP^+ in the HEK empty vector and HEK-OCT1 cells visualized by confocal microscopy; the plot shows the corresponding fluorescence intensity measurements. The effect of the OCT1 inhibitor tetraethylammonium (TEA) in HEK-OCT1 cells is shown by the difference between the central figures and those on the right. (C) Kinetic characterization of ASP^+ uptake in HEK-OCT1 plotted according to the Michaelis−Menten equation (eq 1), which allows the determination of apparent K_m and V_{max} values. The ASP^+-uptake data are normalized to the protein content of the cells.

OCT1 cells constitute a close-to-ideal model for the study of both the transport and the inhibition of OCT1.

The ASP^+ uptake was inhibited by tetraethylammonium (TEA), a known OCT1 inhibitor (Figure 1b). The visualization of the ASP^+ uptake in OCT1 and in vector-transfected cells by confocal microscopy corresponded to the uptake rates (see Figure 1b). The uptake of 1 μM ASP^+ was linear ($r^2 = 0.97$) for up to 15 min, and the apparent K_m (the apparent affinity of ASP^+ for OCT1) and V_{max} (maximal turnover rate of ASP^+ by OCT1) values were determined to be 2.32 ($\pm$0.29) μM and 696 ($\pm$198) RFU/min/mg protein, respectively (Figure 1c). The final assay setup revealed a coefficient of variance (CV) of 11% for the mean values of the transport rates between different experiments and of 15% or less within single plates. Furthermore, the assay had a Z value of 0.78 (an ideal assay has a Z value of 1, whereas for an excellent assay, $1 > Z > 0.5$), which implies that our assay setup is suitable for screening purposes.[17]

Characteristics of the Data Set. The data set that was used in this study ($n = 191$) was composed of compounds that mainly described the oral drug space and compounds that were known to or predicted to interact with OCT1 (Figure 2). (Except for drugs administrated orally, a few drugs administrated via other routes, e.g. via injection or inhalation, were also included in the data set.) The distribution of the data set in the structural space of oral drugs is visualized in Figure 3. The data set was also heterogeneous with regard to size, lipophilicity, and charge (Figure 4a−c). The molecular weight distribution in the data set ranged from 8 (lithium) to 1449 (vancomycin), with a mean of 330.4 $\pm$ 12.5 g/mol, which thoroughly covers the range of conventional marketed drugs.[14] The ClogP values ranged from −4.16 to 6.25 (with the mean value being 1.98 $\pm$ 0.16), the mean polar surface area was 79.0 $\pm$ 4.9 Å^2, and the nonpolar surface area was 303.5 $\pm$ 11.9 Å^2 in this data set (Table 2). Furthermore, the data set included positively charged (42%), neutral (45%), and as negatively charged (13%) compounds (Figure 4c). The low percentage of negatively charged compounds in the data set is due to the fact that only a few negatively charged compounds are found among known OCT1 inhibitors and hence also among compounds that were obtained from the structural similarity search.

Physicochemical Properties of the OCT1 Inhibitors. Using a cutoff value of 50% inhibition of the ASP^+ transport (Table 1, Figure 5), we identified 62 (32%) of the 191 compounds to be inhibitors of OCT1; as many as 47 of these have not previously been reported. We superimposed the inhibitors and noninhibitors on the oral drug space to obtain an overview of the physiochemical properties that influence the inhibition of OCT1. In Figure 6a, the most important molecular properties that were found for all of the investigated drugs were projected in a principal component analysis (PCA). The first principal component (represented on the x axis in Figure 6a) is largely governed by the molecular size, which increases to the right. The second principal component (y axis in Figure 6a) is mostly governed by the hydrophobicity, which increases toward the bottom of the graph. The identified inhibitors are clustered in the middle of the plot, which shows that they are of average size compared with orally administered drugs. Indeed, the molecular-weight range of the inhibitors is 179−531 g/mol with an average of 336 $\pm$ 9.3 g/mol, which is similar to the mean values of both noninhibitors and of all screened compounds (Table 2). Therefore, molecular size per se was not a discriminating factor for OCT1 inhibition. The distribution of the inhibitors along the negative part of the y axis (Figure 6a) indicated that they were hydrophobic, which is also evident

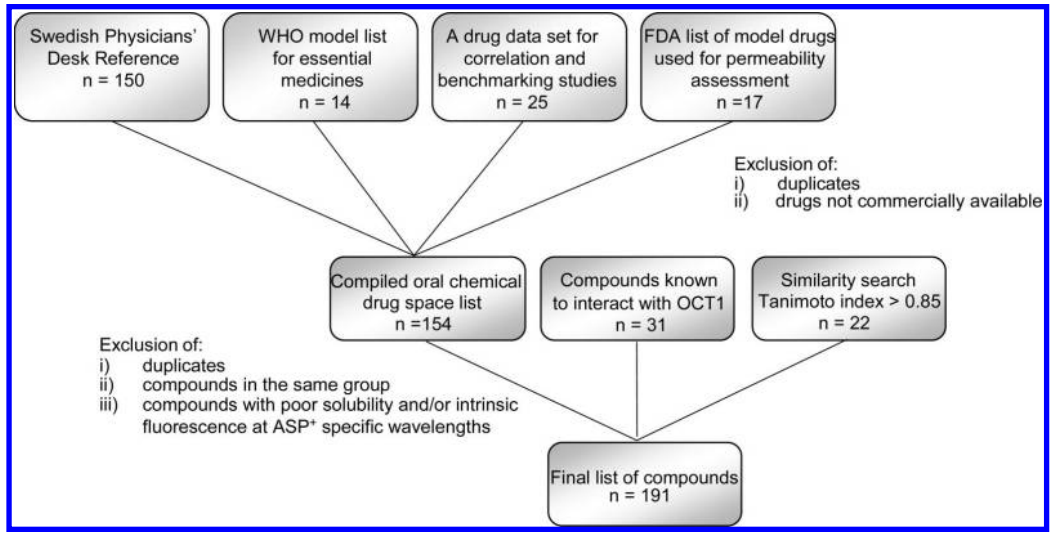

Figure 2. Schematic representation of the selection of the data set. The reduction of the total number of compounds at each level was a result of the listed exclusion criteria.

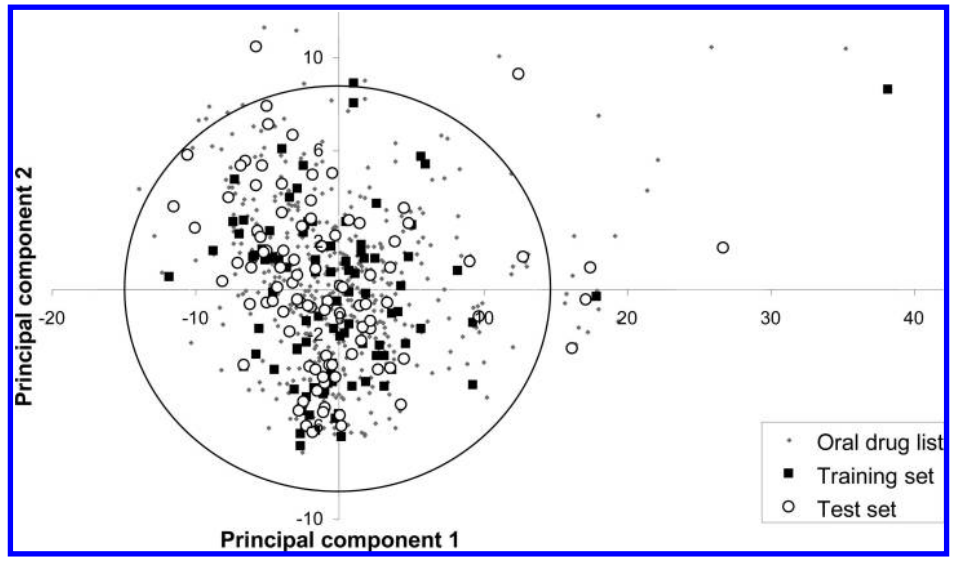

Figure 3. Principal component analysis (PCA) of all oral drugs registered in Sweden (gray dots) and of compounds investigated in this study, which are divided into training (■) and test sets (○). The compounds were chosen to cover the structural oral drug space. The circle shows the 95% confidence interval of the PCA, and principal component 1 mainly reflects compound size (increasing to the right), whereas principal component 2 mainly reflects hydrophobicity (increasing toward the bottom of the graph).

when the hydrophobicity of the inhibitors and noninhibitors is compared in Table 2.

Figure 6b and Table 2 demonstrate that the inhibitors have higher lipophilicities than the noninhibitors with a mean ClogP value of 3.50 (±0.17) compared with 1.43 (±0.19) for the noninhibitors and 1.98 (±0.16) for the whole data set. The only outlier among the inhibitors is the hydrophilic drug amiloride (ClogP = −1.67), which inhibited ASP^+ uptake by 69%. In the absence of high lipophilicity, the inhibitory potential of amiloride, a known OCT1 inhibitor,[18] may be determined by its positive charge at physiological pH and by the large number of positive ionizable groups in the amiloride molecule.

Of all identified inhibitors, 66% carried a positive charge at physiological pH, 32% were neutral, and only one OCT1 inhibiting compound was anionic, namely, the oral antidiabetic compound repaglinide (Figure 6c, Table 1). Furthermore, the OCT1 inhibitors had low polarities, and hydrogen bond donors and acceptors were less frequent than they were in noninhibiting compounds.

Model Development. The experimental results were used to develop qualitative computational models that discriminated the inhibitors from the noninhibitors. In the first step, we only used the important physicochemical characteristics that were identified in the previously described analysis, that is, the hydrophobicity, the lipophilicity, and the charge (Table 2). Therefore, three molecular descriptors representing each of these three physicochemical properties (Nonpolar count/M_w, ClogP, and positive ionizability, respectively) were used in the first attempt at modeling OCT1 inhibition. The resulting qualitative model performed surprisingly well and correctly predicted 75 and 78% of the inhibitors and noninhibitors in the test set, respectively (Figure 7a).

To enhance model performance, we developed a second model in which additional molecular properties were included. In this discriminant model, 93 molecular descriptors that represented the molecular size, flexibility, connectivity, polarity, charge, and hydrogen-bonding potential provided the starting point. After the model refinement process, the final model was based on the 10 most important descriptors. These represent four main property

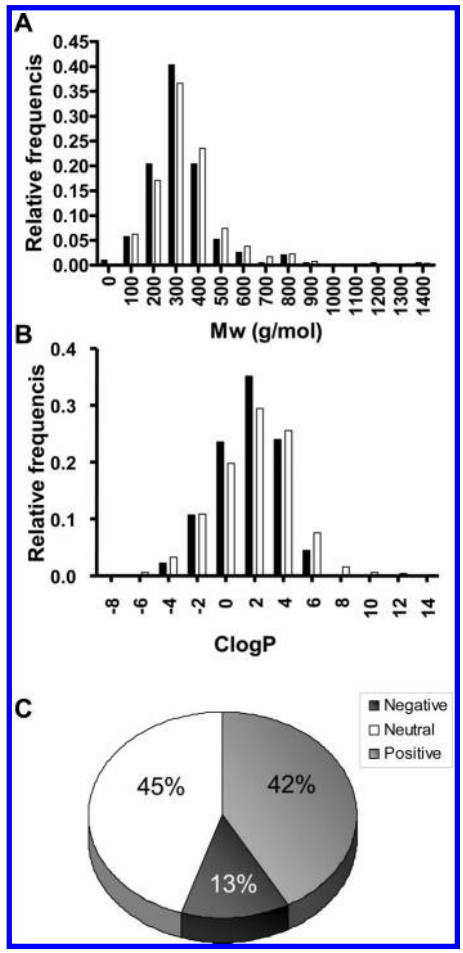

Figure 4. Molecular characteristics of the data set that was used in this study (closed bars) compared to a data set that is composed of all oral drugs registered in Sweden (open bars) in A and B. (A) Distribution of molecular weight, (B) lipophilicity, and (C) charge of the data set.

groups: (i) lipophilicity and hydrophobicity measures (calculated log P and nonpolar count/M_w) with a positive correlation to OCT1 inhibition, (ii) charge (negative ionizability) with a negative correlation to OCT1 inhibition, (iii) hydrogen bonding (minimum distance between hydrogen-bond donor and acceptor functionalities and the sum of all hydrogen-bond donor energies) with the presence of many and strong hydrogen bonds negatively correlating to inhibition, and (iv) dipole properties (average positive charge (Gasteiger), charge range (Gasteiger and Hückel), and average negative charge (Gasteiger and Hückel)) with a negative correlation to OCT1 inhibition. The correlation and relative importance of the 10 molecular descriptors are shown in Figure 8b. The qualitative model performed extremely well and correctly predicted 82% of the inhibitors and 88% of noninhibitors in the test set (Figure 8a).

Discussion

In this study, we developed a simple, fast, and reliable screening method to examine OCT1 transport, and we used this method to investigate the oral drug space with regard to the inhibition of OCT1. To our knowledge, this is the most extensive investigation of OCT1 inhibitors that has been presented, and the size and diversity of the data set facilitated the examination of the molecular properties that contribute to the drug inhibition of OCT1 transport. Previous reports on the inhibition of OCT1 have used different substrates and different concentrations of the test compounds, which makes it very difficult to make meaningful comparisons between the results.[4,11,12] As a result of this, we decided to apply a higher cutoff limit for defining compounds to be inhibitors. Therefore, 50% inhibition of the ASP^+ transport at an inhibitor concentration of 100 μM, was required for classification as an inhibitor, which makes the influence of day-to-day variation less pronounced and our results sufficiently robust to allow qualitative computational modeling. Another potentially confounding factor in the study of OCT1 was that rat and human orthologs to OCT1 may be bidirectional transporters that are primarily driven by the substrate concentration.[7] However, in our new assay, we prevented bidirectional transport by excluding the postincubation wash and by reading the intracellular concentration of the fluorescent ASP^+.

We identified 62 OCT1 inhibitors, of which as many as 47 have not been reported before. The data set we investigated was designed to include previously reported OCT1 inhibitors, which were independent of the method and concentration that had been used when they were initially identified. The reason why only 15 of the 34 known inhibitors were defined as inhibitors in our assay can largely be explained by the fact that many of these exhibit only minor inhibitory effects[11,19] or they were tested at concentrations over 100 μM (the concentration used in this study) in earlier studies. However, four compounds (corticosterone, famotidine, indinavir, and ranitidine) that were previously reported to inhibit OCT1 at low concentrations[11,12,20,21] did not inhibit ASP^+ uptake above the cutoff of 50% that was used in our assay and were, therefore, not considered to be inhibitors. These four compounds inhibited the ASP^+ transport to between 29 and 43% and would therefore have been identified as inhibitors had a less-stringent inhibition criterion been used. The most likely explanation of the observed discrepancy is that the model substrates that were used in the different studies display different sensitivities to the inhibitors. We note that most of the identified inhibitors have a long history of safe use in patients. This suggests that in most cases OCT1 inhibition will have limited effects on systemic drug exposure. The significance of inhibition can be enhanced in patient subpopulations that express genetic variants of OCT1 with reduced function, as was recently reported for the common antidiabetic drug metformin.[22]

We observed that a number of therapeutic classes contained large proportions of inhibitors (Supporting Information, Table S2). The most evident example is that of the tricyclic antidepressants (TCAs), all of which exhibited an inhibition of >77%. The tricyclic moiety of the TCAs seems to be important in OCT1 inhibition because structurally similar drugs that were used for the treatment of psychosis and depression were also found to have a high inhibition of the OCT1-mediated transport. In this pharmacological group, chlorpromazine, fluphenazine, flupentixol, chlorprotixene, and prochlorperazine, all of which contain a phenothiazin moiety, inhibited OCT1 (Figure 9). Two compounds with polycyclic ring systems, clozapine and mianserin, were not classified as inhibitors because of our strict cutoff limit of 50% inhibition, but they fell just below this value (48% for both) (Figure 9). The pharmacological mechanism of the OCT1-inhibiting CNS drugs is the inhibition of different neurotransmitter receptors,[23,24] including the dopamine and serotonin receptors. Interestingly, neurotransmitters are substrates for human OCT2 and 3[25,26] and rat OCT1,[27] which share several substrates and inhibitors with human OCT1.[2] OCT1 is also expressed in the brain,[2,5] but whether it plays a role as a neurotransmitter uptake transporter in the human brain remains to be seen. Other pharmacological classes that were enriched

Table 1. Percentage Inhibition,[a] Charge,[b] and Lipophilicity[c] for all Compounds Analyzed in the OCT1 Assay

compd	inhibition (%)	charge at pH 7.4	ClogP	compd	inhibition (%)	charge at pH 7.4	ClogP
spironolactone[d,e]	87.9	neutral	2.94	cisplatin	22.3	neutral	−1.68
verapamil[e]	86.4	+	4.35	levodopa	21.7	neutral	−2.52
doxazosin[d,e]	85.6	neutral	2.16	choline	21.3	neutral	
clomipramine[d,e]	85.3	+	5.45	ofloxacin[e]	21.1	neutral	0.58
chlorpromazine[e]	85.1	+	4.84	antipyrine[e]	20.7	neutral	1.96
bucindolol[d]	84.6	+	2.91	baclofen[e]	20.7	neutral	0.07
desipramine	84.3	+	3.67	ampicillin	20.3	−	−0.73
propafenone[d]	83.8	+	3.54	carisoprodol[e]	19.8	neutral	2.41
β-estradiol[e]	83.5	neutral	4.25	metformin	19.6	+	−0.75
imipramine[d,e]	82.8	+	4.81	valproic acid	19.6	−	2.98
ketoconazole[d,e]	82.3	neutral	3.25	clindamycin[e]	19.5	+	1.74
trihexyphenidyl[d]	79.4	+	4.64	neostigmin	19.4	neutral	1.78
nandrolon[d]	79.3	neutral	3.35	pilocarpine[e]	17.0	neutral	1.22
promazine[d,e]	79.2	+	4.22	ergotamine[e]	16.7	neutral	3.51
clemastine[d]	78.8	+	4.72	meclizine[e]	16.4	+	5.83
amitriptyline[d,e]	78.5	+	5.14	isoproterenol (+)−bitartrate *R* (−)	15.6	+	−0.62
methoxyverapamil (±)[d]	78.1	+	4.11	acetylcysteine	15.5	−	−0.91
orphenadrine[d]	77.6	+	3.89	felodipine	15.5	neutral	2.70
gugglesteron[d,e]	77.5	na[f]	3.58	gabapentin[e]	15.1	neutral	−0.28
trimipramine[d]	77.2	+	5.30	enalapril[e]	14.6	−	0.23
terazosin[d]	77.0	neutral	1.43	tinidazole	14.2	neutral	0.26
atropine[e]	76.5	+	1.67	erythromycin	14.0	+	3.07
repaglinide[e]	76.4	−	4.98	*N*1-methylnicotinamide[e]	13.9	neutral	−0.38
oxybutynin[d]	75.7	+	4.78	glucosamine	13.9	+	−3.12
2-methoxyestradiol[d,e]	74.3	neutral	4.16	famotidine[e]	13.9	+	0.01
fentanyl[d]	73.6	+	3.94	bendroflumetazide	13.7	neutral	1.79
loperamide[d]	73.4	+	3.66	*N*-acetylprocainamide[e]	13.7	+	1.31
tamoxifen[d]	72.1	+	6.24	creatinine	13.3	neutral	−1.12
promethazine[d]	71.1	+	4.42	levothyroxine[e]	12.7	neutral	4.88
flupenthixol[d]	71.0	+	4.33	metaproterenol[e]	12.6	+	−0.62
clotrimazole[d,e]	69.3	neutral	5.44	dopamine	11.8	+	−0.73
apomorphine[d]	69.0	+	3.02	furosemide	11.7	−	1.99
disopyramide[e]	68.8	+	3.57	methimazole	11.6	neutral	−0.51
amiloride	68.7	+	−1.67	ganciclovir	10.5	neutral	−2.55
amsacrine[d,e]	68.4	neutral	3.08	tetracycline[e]	10.4	neutral	−0.07
morphine[d]	67.9	+	1.29	carbamazepine	8.4	neutral	3.00
haloperidole[d]	67.1	+	3.65	cimetidine[e]	8.1	+	0.25
prochlorperazine[d,e]	66.5	+	4.51	allopurinol[e]	7.7	+	−0.84
papaverin[d]	66.3	neutral	3.08	celecoxib	7.7	neutral	4.37
diltiazem[d]	65.5	+	2.62	etoposide	7.5	neutral	1.33
clonidine	65.4	+	2.43	paclitaxel	7.1	neutral	3.64
terfenadine[d]	65.4	+	5.84	vancomycin[e]	7.1	neutral	0.96
chlorprothixene[d]	65.4	+	5.18	chlorzoxazone[e]	6.8	neutral	2.14
androstene-dione[d]	65.1	neutral	3.22	hydralazine	6.5	neutral	0.66
ondansetron[d]	63.8	neutral	2.52	candesartan	6.3	−	3.92
quinidine	62.9	+	2.88	ibuprofen	6.3	−	3.98
fluphenazine[d,e]	61.9	+	4.05	clodronic acid	5.6	−	−0.14
cyproterone[d,e]	61.6	neutral	2.78	eflornithine	5.5	neutral	−2.50
oxprenolol[d]	61.5	+	2.17	pravastatin	5.0	−	1.28
quinine[e]	60.2	+	2.79	diazepam[e]	5.0	neutral	2.93
tramadol[d,e]	60.2	+	2.73	zidovudine	4.7	neutral	0.32
mepenzolate[d]	59.5	neutral	2.84	cyclophosfamide[e]	4.7	neutral	0.63
memantine[d,e]	58.6	+	3.21	arcaine[e]	4.5	+	−2.28
trimethoprim[d,e]	58.1	neutral	1.53	azathioprine	4.2	neutral	0.92
phenoxybenzamine[e]	56.7	neutral	4.54	histamine[e]	4.1	+	−1.09
progesterone	55.7	neutral	3.62	warfarin	4.0	−	2.63
prazosin[e]	55.6[a]	neutral	1.87	acarbose	3.9	+	−3.36
propranolol[d,e]	55.4	+	2.56	cyclosporin A	3.5	neutral	2.92[g]
metoclopramide[d]	52.3	+	1.85	terbutaline[e]	2.6	+	0.17
citalopram[e]	52.0	+	3.24	cysteamine	2.4	neutral	−0.25
loratadine[d,e]	51.8	neutral	4.96	agmatine	2.1	+	−1.97
denopamine[d,e]	51.5	+	1.75	zanamivir[e]	2.0	neutral	−4.16
mianserin[e]	48.4	+	4.25	vinblastine	1.9	neutral	2.19
troglitazone[e]	48.2	neutral	5.61	chloramphenicol[e]	1.4	neutral	0.85
clozapine	47.5	+	3.64	5-fluorouracil[e]	0.9	neutral	−0.81
digoxin[e]	46.9	neutral	1.72	captopril[e]	0.4	−	0.36
chloroquine	46.0	+	4.20	glybenclamide[e]	0.3	−	3.94
scopolamine	43.9	neutral	0.63	fenofibrate	0.2	neutral	5.26
ipratropium[e]	43.4	neutral	2.25	melagatran	−0.2	neutral	−2.32
indinavir	43.0	neutral	3.58	lithium[e]	−0.3	neutral	−0.15
acebutolol[e]	40.9	+	2.31	mannitol	−1.4	neutral	−2.05
naltrexone	40.3	+	1.47	caffeine[e]	−1.4	neutral	−0.06
risperidone[e]	39.3	+	3.41	cephalexin[e]	−1.9	−	−0.99
codeine[e]	39.1	+	1.86	phenytoin	−2.0	neutral	2.05

Table 1. Continued

compd	inhibition (%)	charge at pH 7.4	ClogP	compd	inhibition (%)	charge at pH 7.4	ClogP
timolol[e]	39.0	+	1.90	lidocaine	−2.3	+	2.46
budesonide[e]	38.2	neutral	2.07	normetanephrine (±)	−2.4	+	−0.57
labetalol[e]	38.1	+	1.58	sulfasalazine[e]	−3.7	−	2.98
efavirenz[e]	37.0	neutral	4.48	diclofenac	−3.7	−	4.73
flutamide	34.1	neutral	3.23	nicotine[e]	−3.7	+	1.30
corticosterone[e]	33.5	neutral	2.03	acyclovir[e]	−3.9	neutral	−2.42
folic acid[e]	33.0	−	−2.09	theophylline	−4.4	neutral	−0.34
metoprolol	32.4	+	1.87	atenolol	−4.6	+	0.74
colchicine	31.9	neutral	1.55	cetirizin	−4.8	neutral	2.96
amantadine[e]	31.8	+	1.77	acetylsalicylic acid	−5.7	−	1.02
sotalol	31.8	+	0.76	phenobarbital	−6.0	neutral	1.31
esmolol[e]	31.2	+	1.58	methyldopa[e]	−7.2	neutral	−1.27
epinephrine (−)	29.1	+	−1.27	probenecid	−8.9	−	2.11
ranitidine	28.8	+	0.83	paracetamol[e]	−9.2	neutral	0.47
doxycycline	27.4	neutral	−0.16	ketoprofen	−9.4	−	3.67
sulindac	27.1	−	2.60	hydrochlortiazide[e]	−9.8	neutral	−0.03
procainamide	26.5	+	1.14	pancuronium[e]	−10.3	neutral	4.20
methotrexate[e]	26.3	−	−2.27	glipizide	−12.7	−	2.96
rifampicin	26.2	neutral	5.75	aluminum	−13.5	−	−1.75
buspirone	24.7	+	2.02	propofol	−17.9	neutral	4.47
prednisone	23.3	neutral	1.38	sodium taurocholate[e]	−19.1	−	2.81
simvastatin[e]	22.6	neutral	4.84				

[a] All compounds were analyzed at 100 μM except for prazosin, which was analyzed at 10 μM due to solubility problems. [b] At the physiological pH derived from the predicted pK_a values for the compounds (ADMET Predictor, SimulationsPlus, Lancaster, CA). [c] Represented by ClogP values (SELMA, AstraZeneca, Mölndal, Sweden). [d] Previously unknown OCT1 inhibitors. [e] Compounds included in the training set. [f] na is not available. [g] logP for cyclophilin A.[51]

Table 2. Important Physiochemical Parameters for the Different Groups Used in the Assay[a,b]

property	inhibitors (n=62)	noninhibitors (n=129)	all screened (n=191)	significance inhibitor vs noninhibitor
ClogP	3.5 (0.17)	1.43 (0.19)	1.98 (0.16)	[c]
percent positive charge	67	30	42	na[d]
polar count/M_w (10^{-3})	9.9 (0.6)	16.8 (0.6)	14.6 (0.5)	[c]
nonpolar count/M_w (10^{-3})	50.4 (1.4)	31.3 (1.5)	37.3 (1.3)	[c]
mol wt	335.7 (9.3)	328.0 (17.7)	330.4 (12.5)	ns[e]
polar surface area	42.9 (4.0)	95.5 (6.4)	79.0 (4.9)	[c]
nonpolar surface area	356.5 (11.0)	279.2 (16.2)	303.5 (11.9)	[f]
hydrogen bond donors	1.07 (0.18)	2.66 (0.23)	2.16 (0.18)	[c]
hydrogen bond acceptors	3.38 (0.23)	5.09 (0.31)	4.55 (0.23)	[c]

[a] Represented as mean (±SE). [b] Most of the parameters are significantly different between the inhibitors and the non-inhibitors. [c] $p < 0.001$. [d] na is not applicable. [e] ns is not significant. [f] $p < 0.01$.

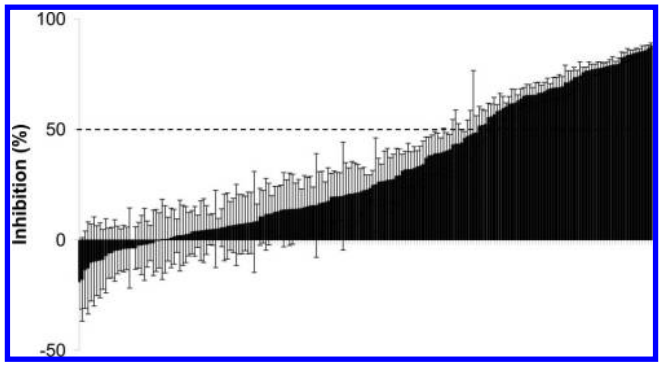

Figure 5. Overview of the results from the screening of OCT1 inhibition. Each bar represents one point in the data set ($n = 191$). At least 50% inhibition (dashed line) was required for a drug to be classified as an inhibitor. The data are presented as mean values ± deviations ($n = 3$).

in OCT1 inhibitors were antihistamines, steroids, and α-receptor blocking agonists. However, further mechanistic studies are needed to address the relevance of these findings.

The unique data set that was obtained in this study allowed us to develop two accurate qualitative computational models for the prediction of OCT1 inhibitors. The model development using orthogonal partial least-squares projection to latent structures discriminant analysis (OPLS-DA) proved to be a powerful tool for the identification of new OCT1 inhibitors and correctly predicted 82% of the inhibitors and 88% of the noninhibitors in the test set of the model based on 10 molecular descriptors (Figure 8). Additionally, an easily interpretable model that uses only three descriptors was generated (Figure 7). This model correctly classified 75% of the inhibitors and 78% of the noninhibitors in the test set and has the advantage of being more transparent than the refined model. The transparency and acceptable performance of the latter model may be valuable for rapid interpretation early in the drug discovery process.

A similar approach was recently used in studies of the efflux transport proteins BCRP (ABCG2) and MRP2 (ABCC2), which suggests that our strategy may be generally applicable to the transporter field.[28,29] The most important molecular features for OCT1 inhibition, according to our data, were hydrophobicity, which had already been suggested as an important feature for a smaller and more homogeneous data set ($n = 30$) by Bednarczyk and coworkers;[11] lipophilicity, which is known to be important for transport-protein inhibition;[28,30] and positive charge, which has previously been reported to be an important feature for OCT1 interaction.[2,31] Features that correlate to a lack of inhibition of the OCT1-mediated transport were also identi-

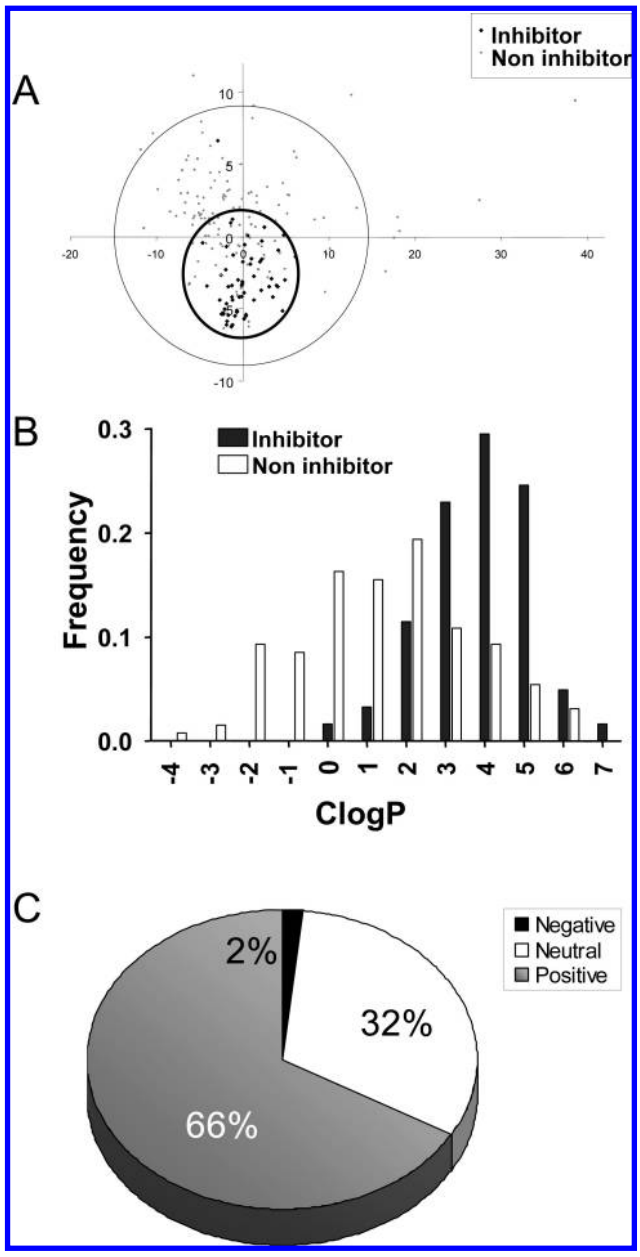

Figure 6. (A) PCA of physiochemical properties of the compounds screened. The gray dots represent the noninhibitors analyzed in this study; the black diamonds represent the inhibitors. The first principal component shows the size of the molecules, which increases to the right, and the second component represents the hydrophobicity, which increases toward the bottom of the graph. The inhibitors have a similar size distribution but show a higher hydrophobicity than the noninhibitors. The outer circle defines the 95% confidence interval of the PCA. (B) ClogP distribution of the inhibitors and noninhibitors (black and white bars, respectively). The OCT1 inhibitors were more lipophilic than the noninhibitors. (C) Charge distribution of the compounds identified as inhibitors in this study. Two-thirds of the inhibitors are cations at physiological pH. Repaglinide, an oral antidiabetic drug, is the only negatively charged compound that inhibits OCT1.

fied. High values in polarity and the existence of many hydrogen-bond donor and acceptor moieties were clearly overrepresented among the compounds that did not inhibit OCT1.

The finding that lipophilicity and charge distribution were important in the inhibition of OCT1 suggests that the interaction with the lipophilic and negatively charged cell membrane may be a crucial step in achieving OCT1 inhibition. The absence of hydrogen-bonding moieties is a significant feature for OCT1

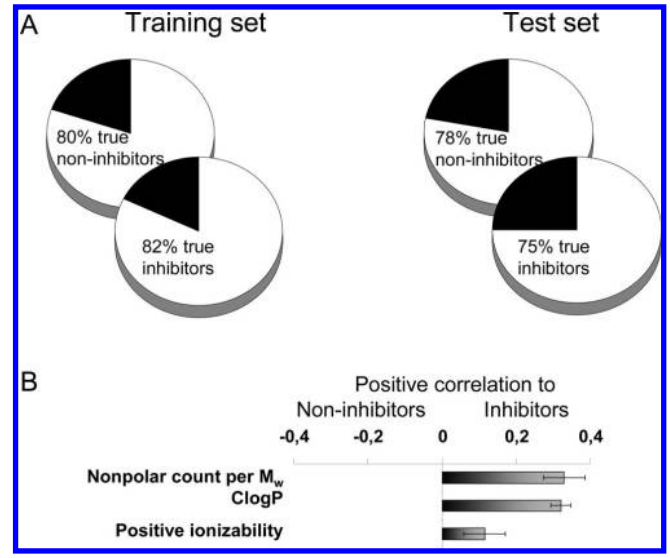

Figure 7. (A) Performance of the easily interpretable model of OCT1 inhibition based on only three molecular descriptors. The left pie charts show the training-set performance, and the right pie charts show the test-set performance. (B) Relative importance of the three descriptors that were used to develop the model. All three descriptors have positive values, which indicates that they were positively correlated to OCT1 inhibition.

inhibitors, a property that increases the lipophilicity of the compound and thereby further facilitates the interaction with the lipophilic cell membrane.

As is the case for most other drug-transporting membrane proteins, a crystal structure has not yet been obtained for OCT1. Instead, pharmacophore modeling and structure−property-based computational models have been used to model interactions with OCT1[11] and other transporters.[32−34] Therefore, we also applied pharmacophore modeling approaches and quantitative partial least-squares (PLS) analysis. For this purpose, we generated full-inhibition curves for as many as 44 OCT1 inhibitors and calculated IC_{50} (Supporting Information, Table S4) and K_i values. However, neither of the two quantitative model approaches could predict the K_i values for OCT1. A similar difficulty of conducting quantitative predictions of OCT1 inhibition was experienced by Bednarczyk and coworkers, who were unable to rank the predicted IC_{50} values in the same order as the measured ones.[11] We speculate that the inability of our models to predict K_i values correctly is due to the fact that the inhibitors spanned a rather narrow K_i interval of less than two log units and that the modeling approaches were unable to capture such small differences in the structurally diverse data set. The range of IC_{50} for the 44 compounds was 4.9−141.9, and 25 compounds were within the 10−50 μM region. Furthermore, the inhibitory compounds may display more than one type of inhibition. The possibility that there are several inhibition sites has been proposed by homology modeling. Studies on rat OCT1[35] and human OCT2[36] suggested that a large hydrophilic cleft is involved in substrate binding in these structural homologues to human OCT1. The size of the cleft and the spatial separation of amino acids, which are important for substrate binding within the cleft, suggest the possibility of several substrate-binding sites.[35] To obtain preliminary information on the inhibition mechanism of OCT1, we studied 10 of the 62 identified inhibitors by using Cornish-Bowden and Dixon plots,[37,38] which indicate whether an interaction is competitive (data not shown). This investigation indicated that 6 out of the 10 model inhibitors that were analyzed were competitive inhibitors whereas 4 showed possible deviations from the ideal competitive inhibition.

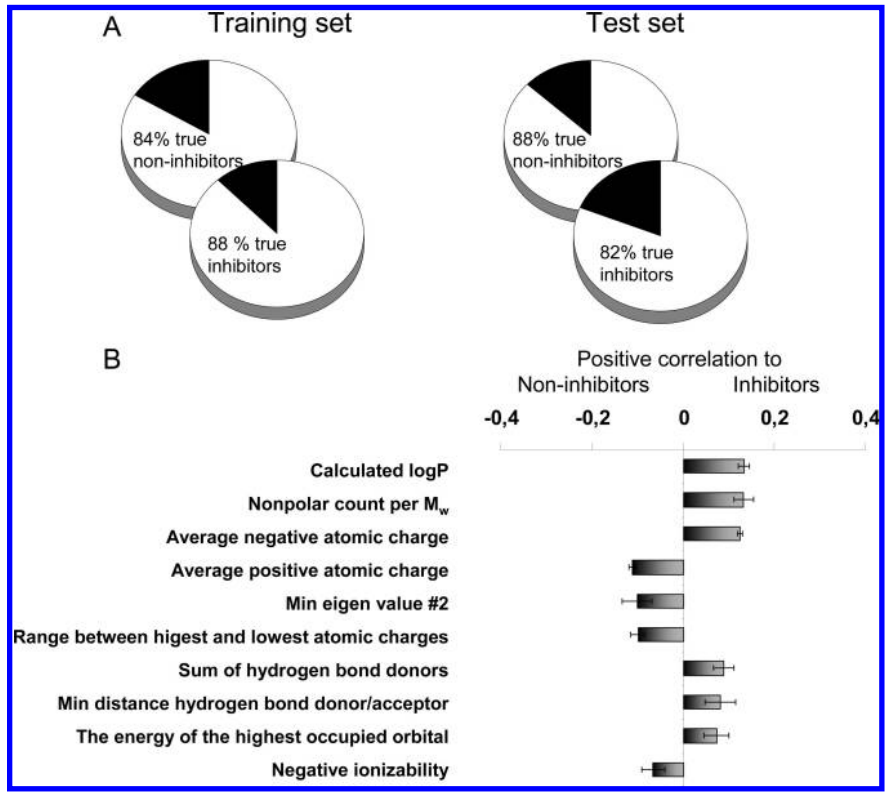

Figure 8. (A) Performance of the model for training and test sets for the more refined model that was described in the text. The left pie charts show training-set performance, and the right charts show the performance for the test set. This model performs better than the easily interpretable model in Figure 7. (B) The 10 molecular descriptors that were used to generate a high-performance model that discriminates between OCT1 inhibitors and noninhibitors. Because the sum of hydrogen-bond donors has a negative value and a positive correlation to OCT1 inhibition, high hydrogen-donor energies in a molecule is, in fact, negatively correlated to inhibition. This is also the case for average negative atomic charge and the energy of the highest-occupied orbital. Compared with the easily interpretable model, this model contains descriptors that are both positively and negatively correlated to OCT1 inhibition.

Therefore, it is possible that different inhibition mechanisms could contribute to our failure to develop quantitative models.

Conclusions

We have developed a sensitive and robust high-throughput assay for the screening of OCT1 inhibitors. The assay was used to measure a large, structurally diverse data set ($n = 191$) for OCT1 inhibition and 47 novel inhibitors were found. High lipophilicity and positive charge were identified as the two main properties that drive OCT1 inhibition, whereas the high dipole moment and the large number of hydrogen bonds of the molecule were negatively correlated to the OCT1 inhibition. The obtained data were used to develop computational models for the prediction of OCT1 inhibitors and correctly predicted 82% of the inhibitors and 88% of the noninhibitors in the test set. We hope that our findings will stimulate the development of predictive transporter-interaction models that are better suited for specific drug discovery programs in which the chemical space differs from that of orally administered drugs.

Materials and Methods

Compounds. A total of 191 compounds were analyzed in the OCT1 inhibition assay. These were obtained from Sigma-Aldrich (St. Louis, MO), International Laboratory USA (San Bruno, CA), 3B Scientific (Libertyville, IL), and AstraZeneca (Mölndal, Sweden). ASP^+ was obtained from Molecular Probes (Carlsbad, CA).

Data-Set Selection. We selected a large and structurally diverse druglike data set to investigate the chemical space of OCT1 inhibitors (Table 1 and Figure 2). This data set was chosen from the Swedish Physicians' Desk Reference,[14] the WHO model list of essential medicines,[39] a drug data set that was proposed for correlation and benchmarking studies,[40] and an FDA list of model drugs that are used for permeability assessment[41] according to the flow chart that is shown in Figure 2. After merging these lists, we excluded duplicates and compounds not being commercially available. This resulted in a data set that was composed of 154 compounds, with a focus on compounds that reach systemic circulation. The data set was supplemented with compounds that had previously been reported to interact with OCT1 ($n = 34$). Finally, a structure similarity search was conducted[42] in which compounds with structural resemblance to previously proposed OCT1-interacting compounds were identified from 1280 compounds from the Library of Pharmacologically Active Compounds (LOPAC; Sigma-Aldrich, St. Louis, MO). Compounds with a Tanimoto similarity index that was above 0.85 ($n = 22$) were included in the list and were investigated in our assay. After a second round of exclusion of duplicated compounds, of compounds for which the predicted or experimental solubility was too poor, and of compounds with an intrinsic fluorescence at ASP^+-specific wavelengths, the final data set was composed of 191 compounds that represented a majority of the different therapeutic groups that were defined in the Swedish Physicians' Desk Reference.[14] To confirm the druglikeness of the final data set, we superimposed the compounds onto the chemical space of oral drugs (Figure 3).

Cell Culture. We studied OCT1-mediated uptake in stably transfected HEK293-OCT1 cells by using HEK293-T-REx empty vector cells as a negative control.[43] The cells were cultivated in 75 cm^2 cell culture flasks (Corning, Corning, NY) in Dulbecco's modified eagle's medium (Invitrogen, Karlsbad, CA) containing 10% fetal bovine serum (Sigma-Aldrich, Saint Louis, MO), 2 mM L-glutamine (GIBCO, Paisley, Scotland), and 500 μg/mL geneticin (GIBCO, Paisley, Scotland). The cells were incubated at 37 °C in an atmosphere of 95% air and 5% CO_2. The cells were subcultured

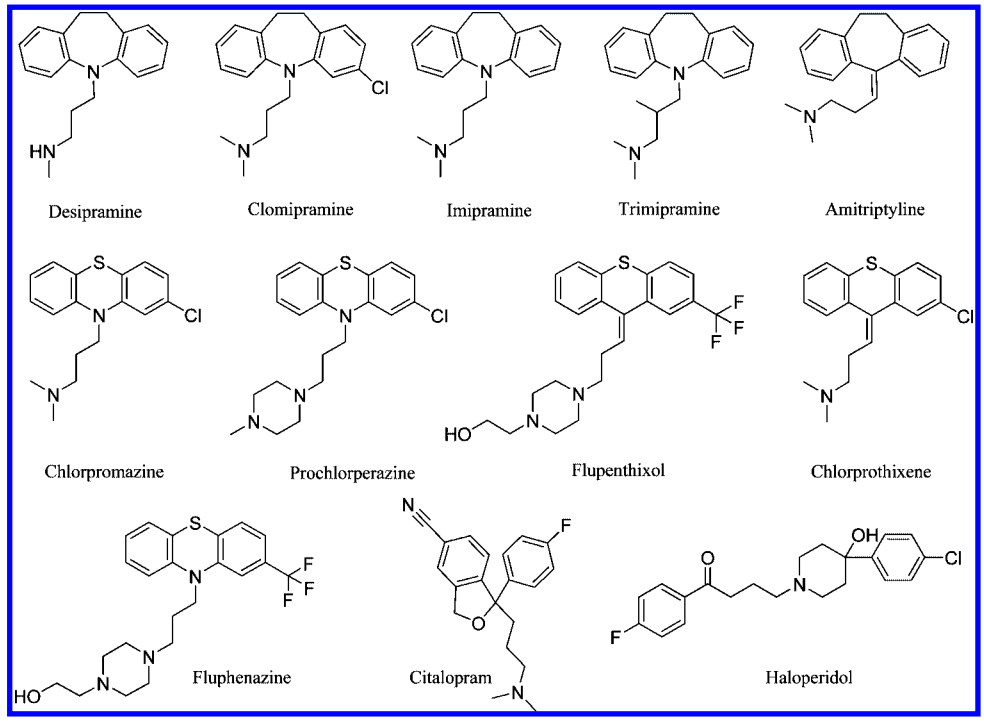

Figure 9. Tricyclic antidepressive drugs and drugs used for the treatment of psychosis and depression that are identified as OCT1 inhibitors. All TCAs inhibited OCT1 by >77%.

twice a week at 70−95% confluence, and passages between 10 and 54 were used in the study.

Gene Expression of Transport Proteins. Real-time PCR (RT-PCR) was used to access the relative gene expression of 10 ABC and 26 SLC transporters. The following transporters, which were selected for their proposed functionality in drug transport, were studied: ABCB1, ABCB4, ABCB11, ABCC1, ABCC2, ABCC3, ABCC4, ABCC5, ABCC6, ABCG2, SLC10A1, SLC10A2, SLC15A1, SLC15A2, SLC16A1, SLC16A4, SLC22A1, SLC22A2, SLC22A3, SLC22A4, SLC22A5, SLC22A6, SLC22A7, SLC22A8, SLC22A9, SLC22A11, SLC28A3, SLC29A1, SLCO1A2, SLCO1B1, SLCO1B3, SLCO1C1, SLCO2B1, SLCO3A1, SLCO4A1, and SLCO4C1. Moreover, six enzymes (CYP1A1, CYP1A2, CYP2D6, CYP2C9, CYP3A4, and CYP3A5) were investigated and were selected on the basis of their importance for drug metabolism.

HEK-OCT1 and HEK empty vector cells were harvested at passages 17 and 18, respectively, and RNA was isolated from the samples by the use of the RNAeasy mini kit (QIAGEN, Hilden, Germany) in accordance with the protocol that was provided from the manufacturer with the addition of an extra on-column DNase (QIAGEN, Hilden, Germany) step. The RNA concentration was measured with a Nanodrop ND-1000 spectrophotometer (Nanodrop, Wilmington, DE), and the RNA quality was examined by the use of a Bioanalyser (Agilent, Palo Alto, CA).

We converted the RNA into cDNA by using the high-capacity cDNA archive kit (Applied Biosystems, Foster City, CA). A 500 ng portion of the total RNA samples was added to a master mixture that contained 10 μL of 10× RT buffer, 4 μL of 25× dNTPs, 10 μL of 10× random primers, 5 μL of Multiscribe RTase (50 U/μL), and 21 μL of nuclease-free water. The reverse-transcriptase PCR mixture was incubated at 25 °C for 10 min and thereafter at 37 °C for 120 min in a Mastercycler gradient system (Eppendorf, Hamburg, Germany). The output cDNA (5 ng/μL) was stored at −70 °C pending RT-PCR analysis.

RT-PCR was carried out as described previously by Hilgendorf et al.[6]

To determine the most suitable internal-reference gene, we used the Excel-based tool BestKeeper.[44] Using this method, we chose a geometric mean of the internal-reference genes PPIA, RPLP0, and MVP as an internal standard. The combined C_t value of these reference genes was extracted from the software, and the relative gene expression was calculated to be $2^{-\Delta C_t}$.[45]

Confocal Microscopy. ASP^+ was used as a model substrate for OCT1.[13,46] ASP^+ is a fluorescent organic cationic mitochondrial dye (excitation 475 nm and emission 605 nm) that fluoresces inside cells but has negligible fluorescence in the extracellular medium. Therefore, the ASP^+ outside the cells does not influence the results. The concentration of ASP^+ that was used in this study (1 μM) is nontoxic to cells, and the compound shows stable fluorescence properties.[47] The ASP^+ influx into HEK cells was visualized by the use of confocal microscopy (Leica, Wetzlar, Germany). OCT1 and empty vector cells were seeded on cover glasses 48 h before they were analyzed. The medium was removed, and the cells were washed once with PBS and were then incubated for 5 min with 1 μM ASP^+, with 1 μM ASP^+ + 3 mM TEA (a known OCT1 inhibitor), or with HBSS only. After the incubation, fluorescence micrographs were obtained (Figure 1b) at ASP^+-specific wavelengths and were analyzed by the use of Leica confocal software (Leica, Wetzlar, Germany).

ASP^+ Transport Kinetics. HEK-OCT1 and HEK empty vector cells were seeded in black 96-well plates that were coated with poly-D-lysine (Greiner, Frickenhausen, Germany) 48 h prior to the experiment at 50 000 cells (100 μL) per well. Directly after seeding the cells, we preincubated the plates at room temperature for 1 h prior to their incubation at 37 °C in 5% CO_2. The intention was to obtain an even cell distribution throughout all wells and to minimize the edge effect.[48] An extra 100 μL of medium was added to the wells after 24 h of cultivation to avoid a nutrient deficit. On the day of the study, the cells were washed twice with 37 °C PBS to remove the cultivation medium. Thereafter, the cell layers were incubated with a solution that contained HBSS and 1−30 μM fluorescent substrate ASP^+. The ASP^+ uptake was monitored at regular time intervals between 1 and 60 min. All samples were run in triplicate at 37 °C. The plates were repeatedly analyzed in a Saphire^2 plate reader (Tecan, Männedorf, Switzerland) at the specific ASP^+ wavelengths. The protein content of each well was measured by the use of a BCA protein assay reagent kit (Pierce Biotechnology, Rockford, IL) to correct the fluorescence data to the number of cells. We assessed the uptake kinetics of ASP^+ by first plotting the initial uptake rates (up to 5 min) against the ASP^+ concentration and then by determining the apparent K_m and V_{max} values by nonlinear regression to the Michaelis−Menten equation (Figure 1, eq 1) by using Prism version 4.02 (GraphPad, San Diego, CA), where v is the uptake rate and S is the substrate concentration.

$$v = \frac{V_{max}S}{K_m + S} \quad (1)$$

OCT1 Inhibition Assay. The test solutions of the 191 compounds that are listed in Table 1 were prepared with a final concentration of 100 μM in HBSS (pH 7.4) and 1 μM fluorescent ASP^+. The test-compound concentration was chosen to be approximately 40 times above the ASP^+ K_m. For compounds that were not soluble at this concentration, DMSO (Sigma-Aldrich, St. Louis, MO) was used as a cosolvent at a final concentration of 1% (v/v), which was nontoxic to the cells and did not affect the transport of ASP^+ (data not shown).

The cells were washed twice with 37 °C PBS, and triplicates were incubated with solutions that contained 1 μM ASP^+ and test compound (100 μM) for 5 min. Wash and incubation steps were carried out in a Freedom EVO200 liquid-handling station (Tecan, Männedorf, Switzerland). Because ASP^+ exhibited negligible fluorescence outside the cells, no postincubation wash was needed (Figure 1b). Another advantage of leaving the excess ASP^+ in the extracellular medium is that it maintains the concentration gradient and reduces any efflux of ASP^+ (data not shown). The plates were analyzed in a Saphire^2 plate reader and were adjusted to read fluorescence inside the cells at the ASP^+-specific excitation (475 nm) and emission wavelength (605 nm). Wells containing HEK-OCT1 cells incubated with ASP^+ alone were used to calculate the inhibitory potential of the tested compound tested. All compounds were analyzed at the ASP^+-specific wavelengths to ensure that the intrinsic fluorescence of each compound did not disturb the assay. Wells containing only HBSS were also included to monitor background fluorescence. We assessed intraplate variability by incubating entire plates with 1 μM ASP^+, and we determined the interplate differences by comparing the ASP^+ values of all plates analyzed (data not shown). We determined the assay sensitivity by calculating the assay Z value (eq 2), which is a measurement of the performance of a screening assay.[17]

$$Z = 1 - \frac{3SD_{sample} + 3SD_{control}}{mean_{sample} - mean_{control}} \quad (2)$$

We defined a compound as an OCT1 inhibitor on the basis of its percentage inhibition of ASP^+ uptake. A cutoff value of 50% inhibition was selected by the use of a Manhattan plot, which identified a statistically significant break in the trend for the data at the 50% inhibition level.

Full inhibition curves were generated by the use of eight concentrations (between 0.5 and 500 μM) of the inhibitors. The data were plotted, and IC_{50} values were calculated by the use of Prism version 4.02.

We investigated the inhibition mechanism by using 10 OCT1 inhibitors. These were investigated at four different inhibitor concentrations (within the interval 1−100 μM) and for three different ASP^+ concentrations (5, 2.5, and 1 μM). We plotted these data in two different ways to determine the principal type of inhibition. First, the ratio of the substrate concentrations to the uptake rates (y) was plotted against the inhibitor concentration (x) (Cornisch-Bowden plot),[37] and second, the reciprocal uptake rates were plotted as a function of inhibitor concentration (Dixon plot).[38]

Physiochemical Properties. The pK_a values were obtained by the use of ADMET Predictor software (SimulationsPlus, Lancaster, CA). We used these values to obtain the charge of the compounds at the physiological pH of 7.4 that was used in this study. Furthermore, 93 commonly used molecular descriptors that represent the molecular size, flexibility, connectivity, polarity, charge, and hydrogen-bonding potential were calculated by the use of the SELMA program (AstraZeneca R&D, Mölndal, Sweden). These descriptors have previously been used by our group when predicting drug solubility, permeability, and transport-protein interactions.[28,29,49,50]

Computational Modeling. The data set was divided into a training set, which was used for model development, and a test set, which was used to validate the final model by listing the compounds in alphabetic order and then assigning every other compound to the test set and the remainder to the training set. This approach resulted in a training set that consisted of 95 compounds (34 inhibitors) and a test set of that consisted of 96 compounds (28 inhibitors). Both sets gave good coverage of the structural space of the complete data set (Figure 3) according to a PCA that was generated with the SIMCA-P+ version 11.5 software (Umetrics, Umeå, Sweden). The molecular weight, the ClogP value, and the charge were also adequately covered by each of the two sets (Figure 4, Table 1).

OPLS-DA, as implemented by SIMCA-P+ version 11.5, was used to obtain computational models for the separation of OCT1 inhibitors from noninhibitors. A variable selection procedure was used in which groups of molecular descriptors that did not contain information that was relevant to the problem (i.e., noise) were removed in a stepwise manner to optimize model performance and to ensure that the obtained model would be transparent. We eliminated descriptors from the model if removing them resulted in improved or unaltered discrimination between inhibitors and noninhibitors in the training set.

Pharmacophore modeling was also used to search for shared structural features of the inhibitors. For this purpose, Catalyst version 4.11 software (Accelrys, San Diego, CA) was used as previously described by Matsson et al.[28]

Acknowledgment. We thank Christina Lohmann for the help in assay development and characterization. This work was supported by AstraZeneca, the Swedish Research Council (Grant 9478), the Knut and Alice Wallenberg Foundation, the Swedish Fund for Research without Animal Experiments, and the Swedish Animal Welfare Agency.

Note Added after ASAP Publication. This manuscript was released ASAP on September 13, 2008 with an error in the title. The correct version posted September 19, 2008.

Supporting Information Available: Relative gene expression for ABC, for SLC transport proteins, and for CYP enzymes in HEK293-OCT1 cells, therapeutic groups containing many OCT1 inhibitors, SMILES of all compounds in the dataset, and IC_{50} values for 44 of the OCT1 inhibitors that were identified in this study. This material is available free of charge via the Internet at http://pubs.acs.org.

References

(1) Neuhoff, S.; Ungell, A. L.; Zamora, I.; Artursson, P. pH-dependent bidirectional transport of weakly basic drugs across Caco-2 monolayers: implications for drug-drug interactions. *Pharm. Res.* **2003**, *20*, 1141–1148.
(2) Koepsell, H.; Lips, K.; Volk, C. Polyspecific organic cation transporters: structure, function, physiological roles, and biopharmaceutical implications. *Pharm. Res.* **2007**, *24*, 1227–1251.
(3) Gorboulev, V.; Ulzheimer, J. C.; Akhoundova, A.; Ulzheimer-Teuber, I.; Karbach, U.; Quester, S.; Baumann, C.; Lang, F.; Busch, A. E.; Koepsell, H. Cloning and characterization of two human polyspecific organic cation transporters. *DNA Cell Biol.* **1997**, *16*, 871–881.
(4) Zhang, L.; Dresser, M. J.; Gray, A. T.; Yost, S. C.; Terashita, S.; Giacomini, K. M. Cloning and functional expression of a human liver organic cation transporter. *Mol. Pharmacol.* **1997**, *51*, 913–921.
(5) Bleasby, K.; Castle, J. C.; Roberts, C. J.; Cheng, C.; Bailey, W. J.; Sina, J. F.; Kulkarni, A. V.; Hafey, M. J.; Evers, R.; Johnson, J. M.; Ulrich, R. G.; Slatter, J. G. Expression profiles of 50 xenobiotic transporter genes in humans and pre-clinical species: a resource for investigations into drug disposition. *Xenobiotica* **2006**, *36*, 963–988.
(6) Hilgendorf, C.; Ahlin, G.; Seithel, A.; Artursson, P.; Ungell, A. L.; Karlsson, J. Expression of thirty-six drug transporter genes in human intestine, liver, kidney, and organotypic cell lines. *Drug Metab. Dispos.* **2007**, *35*, 1333–1340.
(7) Koepsell, H.; Schmitt, B. M.; Gorboulev, V. Organic cation transporters. *Rev. Physiol., Biochem., Pharmacol.* **2003**, *150*, 36–90.
(8) Wang, D. S.; Kusuhara, H.; Kato, Y.; Jonker, J. W.; Schinkel, A. H.; Sugiyama, Y. Involvement of organic cation transporter 1 in the lactic acidosis caused by metformin. *Mol. Pharmacol.* **2003**, *63*, 844–848.
(9) Zhang, S.; Lovejoy, K. S.; Shima, J. E.; Lagpacan, L. L.; Shu, Y.; Lapuk, A.; Chen, Y.; Komori, T.; Gray, J. W.; Chen, X.; Lippard, S. J.; Giacomini, K. M. Organic cation transporters are determinants of oxaliplatin cytotoxicity. *Cancer Res.* **2006**, *66*, 8847–8857.

(10) White, D. L.; Saunders, V. A.; Dang, P.; Engler, J.; Zannettino, A. C.; Cambareri, A. C.; Quinn, S. R.; Manley, P. W.; Hughes, T. P. OCT-1-mediated influx is a key determinant of the intracellular uptake of imatinib but not nilotinib (AMN107): reduced OCT-1 activity is the cause of low in vitro sensitivity to imatinib. *Blood* **2006**, *108*, 697–704.
(11) Bednarczyk, D.; Ekins, S.; Wikel, J. H.; Wright, S. H. Influence of molecular structure on substrate binding to the human organic cation transporter, hOCT1. *Mol. Pharmacol.* **2003**, *63*, 489–498.
(12) Hayer-Zillgen, M.; Bruss, M.; Bonisch, H. Expression and pharmacological profile of the human organic cation transporters hOCT1, hOCT2 and hOCT3. *Br. J. Pharmacol.* **2002**, *136*, 829–836.
(13) Gustavsson, L.; Lohmann, C.; Hollnack, E.; Steinwall, J.; Gelius, B.; Danielsson, J.; Skoging-Nyberg, U.; Wahlberg, J.; Hoogstraate, J. Identification of compounds that interact with the human organic cation transporter 1 (hOCT1). *Drug Metab. Rev.* **2006**, *38*, 117.
(14) FASS, Farmaceutiska Specialiteter i Sverige. *Läkemedelsindustriföreningen*; Stockholm, Sweden, 2007.
(15) Goh, L. B.; Spears, K. J.; Yao, D.; Ayrton, A.; Morgan, P.; Roland Wolf, C.; Friedberg, T. Endogenous drug transporters in in vitro and in vivo models for the prediction of drug disposition in man. *Biochem. Pharmacol.* **2002**, *64*, 1569–1578.
(16) Raggers, R. J.; Vogels, I.; van Meer, G. Upregulation of the expression of endogenous Mdr1 P-glycoprotein enhances lipid translocation in MDCK cells transfected with human MRP2. *Histochem. Cell. Biol.* **2002**, *117*, 181–185.
(17) Zhang, J. H.; Chung, T. D.; Oldenburg, K. R. A simple statistical parameter for use in evaluation and validation of high throughput screening assays. *J. Biomol. Screen.* **1999**, *4*, 67–73.
(18) Wessler, I.; Roth, E.; Deutsch, C.; Brockerhoff, P.; Bittinger, F.; Kirkpatrick, C. J.; Kilbinger, H. Release of non-neuronal acetylcholine from the isolated human placenta is mediated by organic cation transporters. *Br. J. Pharmacol.* **2001**, *134*, 951–956.
(19) Zhang, L.; Schaner, M. E.; Giacomini, K. M. Functional characterization of an organic cation transporter (hOCT1) in a transiently transfected human cell line (HeLa). *J. Pharmacol. Exp. Ther.* **1998**, *286*, 354–361.
(20) Bourdet, D. L.; Pritchard, J. B.; Thakker, D. R. Differential substrate and inhibitory activities of ranitidine and famotidine toward human organic cation transporter 1 (hOCT1; SLC22A1), hOCT2 (SLC22A2), and hOCT3 (SLC22A3). *J. Pharmacol. Exp. Ther.* **2005**, *315*, 1288–1297.
(21) Zhang, L.; Gorset, W.; Washington, C. B.; Blaschke, T. F.; Kroetz, D. L.; Giacomini, K. M. Interactions of HIV protease inhibitors with a human organic cation transporter in a mammalian expression system. *Drug. Metab. Dispos.* **2000**, *28*, 329–334.
(22) Shu, Y.; Sheardown, S. A.; Brown, C.; Owen, R. P.; Zhang, S.; Castro, R. A.; Ianculescu, A. G.; Yue, L.; Lo, J. C.; Burchard, E. G.; Brett, C. M.; Giacomini, K. M. Effect of genetic variation in the organic cation transporter 1 (OCT1) on metformin action. *J. Clin. Invest.* **2007**, *117*, 1422–1431.
(23) Woolf, A. D.; Erdman, A. R.; Nelson, L. S.; Caravati, E. M.; Cobaugh, D. J.; Booze, L. L.; Wax, P. M.; Manoguerra, A. S.; Scharman, E. J.; Olson, K. R.; Chyka, P. A.; Christianson, G.; Troutman, W. G. Tricyclic antidepressant poisoning: an evidence-based consensus guideline for out-of-hospital management. *Clin. Toxicol.* **2007**, *45*, 203–233.
(24) Seeman, P. Atypical antipsychotics: mechanism of action. *Can. J. Psychiatry* **2002**, *47*, 27–38.
(25) Busch, A. E.; Karbach, U.; Miska, D.; Gorboulev, V.; Akhoundova, A.; Volk, C.; Arndt, P.; Ulzheimer, J. C.; Sonders, M. S.; Baumann, C.; Waldegger, S.; Lang, F.; Koepsell, H. Human neurons express the polyspecific cation transporter hOCT2, which translocates monoamine neurotransmitters, amantadine, and memantine. *Mol. Pharmacol.* **1998**, *54*, 342–352.
(26) Grundemann, D.; Schechinger, B.; Rappold, G. A.; Schomig, E. Molecular identification of the corticosterone-sensitive extraneuronal catecholamine transporter. *Nat. Neurosci.* **1998**, *1*, 349–351.
(27) Breidert, T.; Spitzenberger, F.; Gründemann, D.; Schömig, E. Catecholamine transport by the organic cation transporter type 1 (OCT1). *Br. J. Pharmacol.* **1998**, *125*, 218–224.
(28) Matsson, P.; Englund, G.; Ahlin, G.; Bergström, C. A. S.; Norinder, U.; Artursson, P. A global drug inhibition pattern for the human ATP-binding cassette transporter breast cancer resistance protein (ABCG2). *J. Pharmacol. Exp. Ther.* **2007**, *323*, 19–30.
(29) Pedersen, J. M.; Matsson, P.; Bergström, C. A. S.; Norinder, U.; Hoogstraate, J.; Artursson, P. Prediction and identification of drug interactions with the human ATP-binding cassett transporter multidrug resistance associated protein 2 (MRP2; ABCC2). *J. Med. Chem.* **2008**, *51*, 3275–3287.
(30) Zhang, L.; Gorset, W.; Dresser, M. J.; Giacomini, K. M. The interaction of *n*-tetraalkylammonium compounds with a human organic cation transporter, hOCT1. *J. Pharmacol. Exp. Ther.* **1999**, *288*, 1192–1198.
(31) Jonker, J. W.; Schinkel, A. H. Pharmacological and physiological functions of the polyspecific organic cation transporters: OCT1, 2, and 3 (SLC22A1−3). *J. Pharmacol. Exp. Ther.* **2004**, *308*, 2–9.
(32) Ekins, S.; Kim, R. B.; Leake, B. F.; Dantzig, A. H.; Schuetz, E. G.; Lan, L. B.; Yasuda, K.; Shepard, R. L.; Winter, M. A.; Schuetz, J. D.; Wikel, J. H.; Wrighton, S. A. Application of three-dimensional quantitative structure-activity relationships of *P*-glycoprotein inhibitors and substrates. *Mol. Pharmacol.* **2002**, *61*, 974–981.
(33) Penzotti, J. E.; Lamb, M. L.; Evensen, E.; Grootenhuis, P. D. J. A computational ensemble pharmacophore model for identifying substrates of *P*-glycoprotein. *J. Med. Chem.* **2002**, *45*, 1737–1740.
(34) Hirono, S.; Nakagome, I.; Imai, R.; Maeda, K.; Kusuhara, H.; Sugiyama, Y. Estimation of the three-dimensional pharmacophore of ligands for rat multidrug-resistance-associated protein 2 using ligand-based drug design techniques. *Pharm. Res.* **2005**, *22*, 260–269.
(35) Popp, C.; Gorboulev, V.; Müller, T. D.; Gorbunov, D.; Shatskaya, N.; Koepsell, H. Amino acids critical for substrate affinity of rat organic cation transporter 1 line the substrate binding region in a model derived from the tertiary structure of lactose permease. *Mol. Pharmacol.* **2005**, *67*, 1600–1611.
(36) Pelis, R. M.; Suhre, W. M.; Wright, S. H. Functional influence of *N*-glycosylation in OCT2-mediated tetraethylammonium transport. *Am. J. Physiol. Renal Physiol.* **2006**, *290*, F1118–F1126.
(37) Cornish-Bowden, A. A simple graphical method for determining the inhibition constants of mixed, uncompetitive and non-competitive inhibitors. *Biochem. J.* **1974**, *137*, 143–144.
(38) Dixon, M. The determination of enzyme inhibitor constants. *Biochem. J.* **1953**, *55*, 170–171.
(39) WHO model lists of essential medicines, 2005. WHO: Geneva, Switzerland. http://www.who.int/medicines/publications/essentialmedicines/en/.
(40) Sköld, C.; Winiwarter, S.; Wernevik, J.; Bergström, F.; Engström, L.; Allen, R.; Box, K.; Comer, J.; Mole, J.; Hallberg, A.; Lennernäs, H.; Lundstedt, T.; Ungell, A. L.; Karlén, A. Presentation of a structurally diverse and commercially available drug data set for correlation and benchmarking studies. *J. Med. Chem.* **2006**, *49*, 6660–6671.
(41) Waiver of In Vivo Bioavailability and Bioequivalence Studies for Immediate-Release Solid Oral Dosage Forms Based on a Biopharmaceutics Classification System, 2006. FDA. http://www.fda.gov/cder/guidance/3618fnl.pdf.
(42) Willett, P. Similarity-based virtual screening using 2D Fingerprints. *Drug Discovery Today* **2006**, *11*, 1046–1053.
(43) Lohmann, C.; Gelius, B.; Danielsson, J.; Skoging-Nyberg, U.; Hollnack, E.; Dudley, A.; Wahlberg, J.; Hoogstraate, J.; Gustavsson, L. Scintillation proximity assay for measuring uptake by the human drug transporters hOCT1, hOAT3, and hOATP1B1. *Anal. Biochem.* **2007**, *366*, 117–125.
(44) Pfaffl, M. W.; Tichopad, A.; Prgomet, C.; Neuvians, T. P. Determination of stable housekeeping genes, differentially regulated target genes and sample integrity: BestKeeper−Excel-based tool using pairwise correlations. *Biotechnol. Lett.* **2004**, *26*, 509–515.
(45) Livak, K. J.; Schmittgen, T. D. Analysis of relative gene expression data using real-time quantitative PCR and the $2^{-\Delta\Delta C_T}$ method. *Methods* **2001**, *25*, 402–408.
(46) Ciarimboli, G.; Struwe, K.; Arndt, P.; Gorboulev, V.; Koepsell, H.; Schlatter, E.; Hirsch, J. R. Regulation of the human organic cation transporter hOCT1. *J. Cell Physiol.* **2004**, *201*, 420–428.
(47) Magrassi, L.; Purves, D.; Lichtman, J. W. Fluorescent probes that stain living nerve terminals. *J. Neurosci.* **1987**, *7*, 1207–1214.
(48) Lundholt, B. K.; Scudder, K. M.; Pagliaro, L. A simple technique for reducing edge effect in cell-based assays. *J. Biomol. Screening* **2003**, *8*, 566–570.
(49) Bergström, C. A. S.; Wassvik, C. M.; Norinder, U.; Luthman, K.; Artursson, P. Global and local computational models for aqueous solubility prediction of drug-like molecules. *J. Chem. Inf. Comput. Sci.* **2004**, *44*, 1477–1488.
(50) Matsson, P.; Bergström, C. A. S.; Nagahara, N.; Tavelin, S.; Norinder, U.; Artursson, P. Exploring the role of different drug transport routes in permeability screening. *J. Med. Chem.* **2005**, *48*, 604–613.
(51) Taylor, N. E.; Mark, A. E.; Vallat, P.; Brunne, R. M.; Testa, B.; and Van Gunteren, W. F. Solvent dependent conformation and hydrogen bounding capacity of cyclosporin A: evidence from partition coefficient and molecular dynamics simulations. *J. Med. Chem.* **1993**, *36*, 3753–3764.

JM8003152